



www.sciencemag.org/content/351/6268/88/suppl/DC1

Supplementary Materials for Structure of the Sec61 channel opened by a signal sequence

Rebecca M. Voorhees and Ramanujan S. Hegde*

*Corresponding author. E-mail: rhegde@mrc-lmb.cam.ac.uk

Published 1 January 2016, *Science* **351**, 88 (2016)
DOI: 10.1126/science.aad4992

This PDF file includes

Materials and Methods
Figs. S1 to S8
Tables S1 and S2
References
Movie legends S1 and S2

Other Supplementary Material for this manuscript includes the following:
(available at www.sciencemag.org/content/351/6268/88/suppl/DC1)

Movies S1 and S2

Materials and Methods

Plasmids, antibodies, and recombinant protein

An SP64 vector-based construct encoding bovine pre-prolactin (pPL) was modified to contain an N-terminal affinity tag (3xFLAG) and short glycine-serine linker to generate FLAG-pPL. The encoded protein sequence is shown in Fig. S1. The mammalian expression construct for GTPase-deficient Hbs1 (Hbs1-DN) has been described [28], and was purified as before [29]. Antibodies against uL6 (Santa Cruz, anti-L9) and uS9 (Santa Cruz, anti-S16) were purchased, and the antibodies against TRAP α , Sec61 α , Sec61 β and TRAM were characterized previously [30, 11-13]. Anti-Flag affinity resin and 3X Flag peptide were obtained from Sigma.

In vitro transcription, translation, and biochemical characterization

Preparation and purification of stalled ribosome nascent chain (RNC) complexes were performed using minor variations of previously described methods [18,28-31]. All *in vitro* translation reactions used the rabbit reticulocyte lysate system assembled as described before [31]. Canine pancreas derived rough microsomes (RMs) were prepared as described [32]. Analytic translation reactions for biochemical characterization were carried out using ^{35}S -methionine to detect the translated products, while preparative scale reactions for cryo-EM (described below) used unlabelled methionine. The template for *in vitro* transcription of the truncated RNC was prepared by PCR from the FLAG-pPL (or untagged pPL) constructs using a 5' primer preceding the SP6 promoter, and a 3' primer at codon 85 of native pPL. The 3' primer encoded a terminal valine as the 86th amino acid, whose peptidyl-tRNA is relatively resistant to spontaneous hydrolysis. Template for full length products used a 3' primer beyond the native stop codon. PCR products were purified and used for *in vitro* transcription as described [31].

Analytical translation reactions to characterize the FLAG-pPL construct (fig. S2-S4) were typically for 20-30 min at 32°C, with further manipulations and analysis performed on ice unless otherwise indicated. Protease protection of full length products (fig. S2A) used 0.5 mg/ml proteinase K at 0°C as described before [30]. Puromycin treatment (fig. S2B) used 1 mM puromycin for 15 min at 32°C. For photo-cross-linker incorporation, the charged suppressor tRNAs were obtained from tRNA Probes (catalog numbers A12 and A13). They were added to the translation reactions at a final concentration of ~1 μM . For cross-linking, the microsomes were sedimented from the total translation reactions by layering the sample on 100 μl of 25% sucrose (w/v) in 120 mM KOAc, 50 mM Hepes, pH 7.5, 2 mM MgCl₂ and centrifuging for 30 min at 55,000 rpm in a TLA55 rotor. After resuspension in the same buffer without sucrose, the samples were irradiated for 15 min on ice ~10 cm from the light source of a UVP B-100 series lamp (UVP LLC). Immunoprecipitations for Sec61 α and TRAM cross-linked products were as before [33]. The protease-protection assay for insertion into the Sec61 channel (fig. S4) was performed as described previously [12, 13]. Where indicated, deacylation of the tRNA prior to SDS-PAGE was performed by adjusting the sample to pH ~12, incubation for 15 min at 37°C, and neutralization with sample buffer.

Sample preparation for EM analysis

Preparative scale RNC purification for EM analysis utilized rabbit reticulocyte lysate that was first depleted of 80S ribosomes by centrifugation for 75 min at 50,000 rpm in a Beckman TLA55 rotor. The resulting supernatant was used in a 3.5-ml translation reaction containing canine pancreatic rough microsomes at a final A_{280} of ~ 12 . Translation occurs on membrane-bound ribosomes contributed from the microsomes, maximizing translocon engagement. After incubation for 5 min at 32° C to initiate translation, Hbs1-DN was added to ~ 133 nM, and incubated for a further 20 min at 32° C. Note that the Hbs1-DN inhibits ribosome splitting and engagement of the ribosome-associated quality control pathway [31], thereby ensuring a more homogeneous RNC population. The resulting membranes were then pelleted by centrifugation for 20 min at 50,000 rpm in a TLA55 rotor, and resuspended in membrane buffer (50 mM HEPES pH 7.5, 250 mM sucrose, 2 mM MgOAc₂) to one-tenth the volume of the initial translation reaction. Solubilization was carried out by addition of an equal volume of 2x solubilisation buffer (3.5% digitonin, 100 mM HEPES pH 7.5, 800 mM KOAc, 20 mM MgOAc₂, 2 mM DTT) and incubated 10 minutes on ice. Samples were centrifuged for 15 min at 20,000 x g at 4° C to remove insoluble material, and then diluted 10-fold in column buffer (50 mM HEPES pH 7.5, 200 mM KOAc, 15 mM MgOAc₂, 1 mM DTT). Note that the digitonin used throughout the solubilization and purification was purified further from the commercially obtained preparation (from Calbiochem) as described before [34].

Affinity purification was carried out in batch by incubation for 2 hours at 4° C with anti-FLAG resin at a 1:100 ratio. The samples were then transferred to a micro-spin column and washed with ~ 100 volumes (relative to the resin volume) of wash buffer (50 mM HEPES pH 7.5, 200 mM KOAc, 15 mM MgOAc₂, 1 mM DTT, 0.25% digitonin). Samples were eluted by incubation for 30 min at 22° C with 1 resin volume of wash buffer supplemented with 0.2 mg/mL 3X FLAG peptide, separated from the resin by a brief spin of the micro-column, and used immediately for grid preparation. The concentration of ribosomes in this final preparation was ~ 100 nM as judged by A_{260} . No ribosomes were recovered from reactions lacking a tagged nascent chain, verifying specificity of affinity purification.

Grid preparation and data collection

The eluted samples were applied directly to glow-discharged holey carbon grids (Quantifoil R2/2), which had been coated with a ~ 70 Å thick layer of amorphous carbon. Using an FEI Vitrobot, 3 μ L of sample was applied to the grid, followed by a 30 sec incubation at 4° C, 9 sec of blotting, and flash-cooling in liquid ethane. Data were collected on an FEI Titan Krios at 300 KV using FEI's automated single particle acquisition software and defocus values of 2-3.5 μ m. Images were recorded using a back-thinned FEI Falcon II detector at a calibrated magnification of 104,478 (pixel size of 1.34 Å). Individual frames from the detector were recorded as previously described [35].

Image processing

Contrast transfer function parameters were estimated using CTFFIND3 [36], and micrographs that had evidence of astigmatism or drift were discarded. All automated

particle picking, 2D and 3D classifications, and refinements were performed using RELION as described below [37]. Unsupervised 2D class averaging was used to discard any non-ribosome particles, resulting 136,639 ribosome-Sec61 particles. 3D classification was utilized to identify the population of 101,339 ribosome-Sec61 particles containing an unratcheted P-site tRNA as a proxy for presence of the nascent chain. Final 3D refinements of the resulting populations were performed utilizing statistical movie processing [35], and particle polishing [38]. This resulted in a final reconstruction at overall resolution of 3.6 Å using the gold-standard FSC=0.143 criteria [39].

Model building and refinement

The model for the open Sec61 channel was built using the archaeal SecY crystal structure [2] and the model for the idle channel [9]. The four transmembrane helices (6 through 9) of Sec61 α that directly contact the ribosome via their associated cytosolic loops required little to no adjustments, while the remaining 6 helices (1-5, 10) and Sec61 β could be rotated as a unit and fit as a rigid body with minimal adjustments into the observed density. The C-terminus of Sec61 γ required further minor adjustments. After fitting of the Sec61 channel subunits, the remaining additional helical density was fit to the signal helix using a combination of the observed density, the biophysical properties of the surrounding helices, and the favourable localization of polar residues away from the lipid bilayer (fig. S8). Refinement was carried out using REFMAC v5.8 [40] as previously described [41, 42]. Secondary structure restraints were generated in ProSMART [43] and were maintained throughout refinement to prevent over-fitting. Local resolution was calculated using ResMap [44] and all figures were generated using Pymol [45] and Chimera [46].

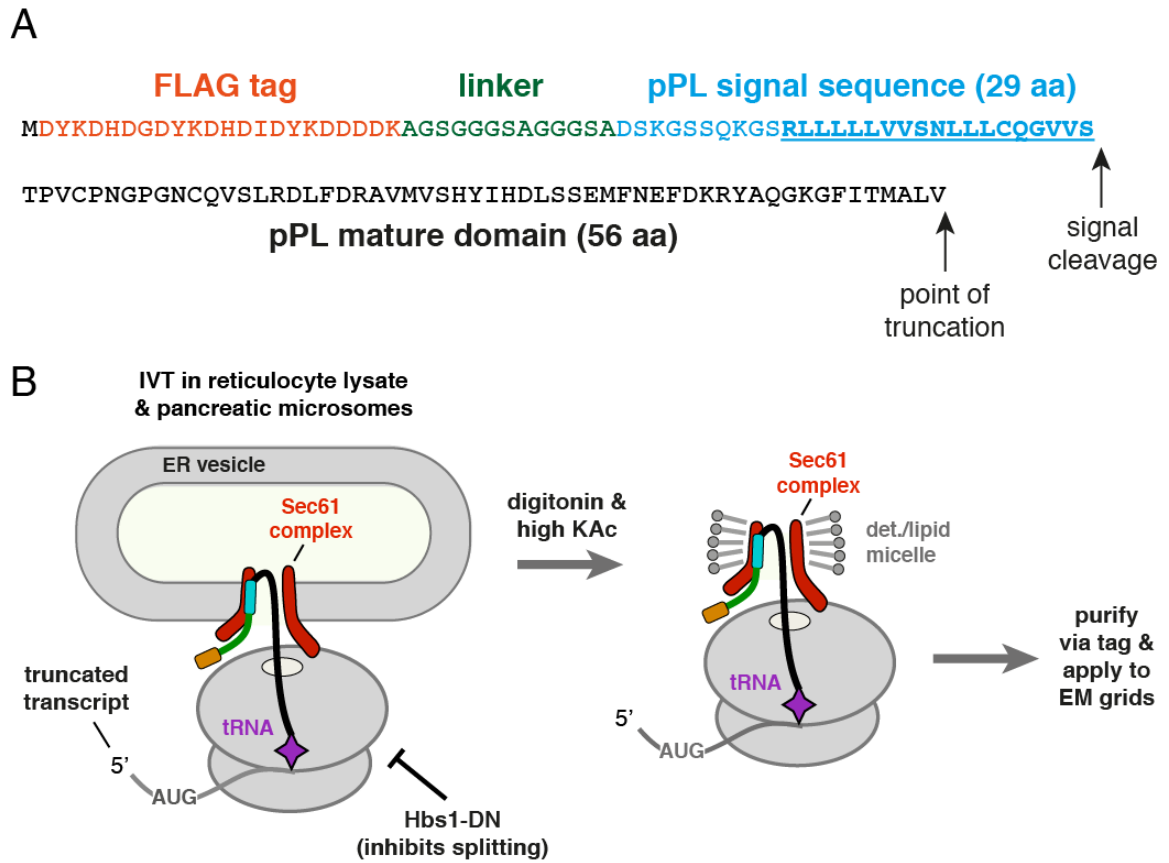


Fig. S1. Experimental strategy for sample preparation. (A) Sequence of the nascent chain used to engage the Sec61 complex. The 3X FLAG tag (orange) and a flexible linker (green) were inserted after the initiating methionine of pre-prolactin (pPL). The signal peptide is in cyan, and the mature domain up to residue 85 of pPL, plus a final valine, is in black. The underlined sequence was modelled in the structure. Extending the pPL signal peptide at the N-terminus is unlikely to affect its function (as verified in Figs. S2 to S4) given that the n-regions of signal peptides are highly diverse and variable in length. (B) Schematic of the translationally stalled substrate bound to the Sec61 complex. As shown in Fig. S2B, this complex is a functional on-pathway intermediate since release with puromycin permits translocation. Note that the GTPase-deficient Hbs1 protein included in the translation reaction prevents ribosome splitting by the ribosome-quality control pathway that ordinarily recognizes stalled ribosomes. Of the 56 residues following the signal peptide, ~35-40 residues are expected to be in the ribosomal tunnel, leaving ~16-21 residues to traverse the Sec61 channel. After assembly, the complex is solubilized using digitonin and high salt, and affinity purified via the FLAG tag before application to EM grids. As shown in Fig. S4, affinity purification does not dislodge the nascent chain from being fully inserted into the Sec61 complex.

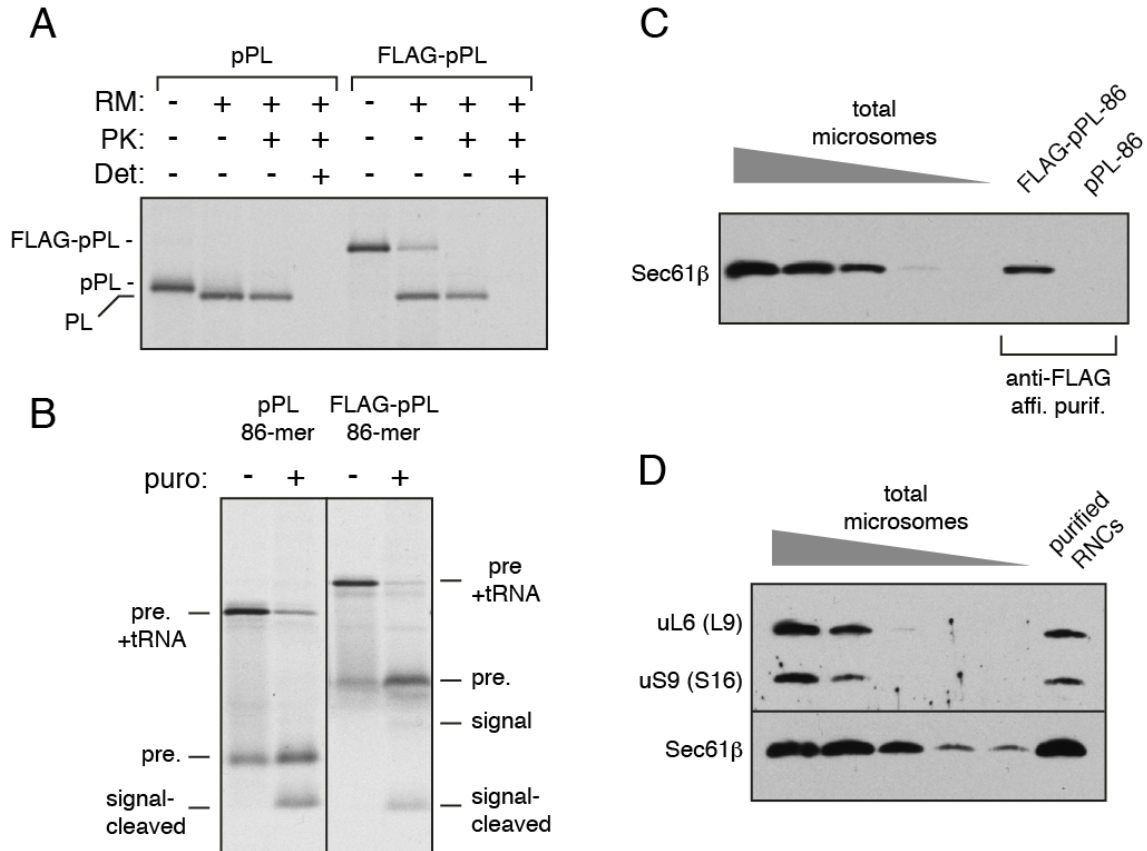


Fig. S2. Biochemical characterization of the FLAG-pPL construct. (A) In vitro translation reactions containing ^{35}S -methionine were programmed with transcripts coding for full length pre-prolactin (pPL) or FLAG-pPL (see Fig. S1). Reactions were performed without or with canine pancreatic rough microsomes (RM) as indicated. After translation, aliquots were digested with proteinase K (PK) in the absence or presence of the detergent (det) Triton X-100 at 0.5%. All samples were analyzed by SDS-PAGE and autoradiography. Note that both pPL and FLAG-pPL are efficiently translocated into microsomes as judged by signal peptide cleavage and protease protection of the processed product. (B) FLAG-pPL or untagged pPL, truncated at residue 86 (numbering of pPL), was translated in the presence of RM and ^{35}S -methionine and either left untreated or reacted with puromycin (puro) before analysis by SDS-PAGE and autoradiography. The positions of the tRNA attached precursor (pre.+tRNA), free precursor (pre.), and signal-cleaved product are indicated. Note that a small amount of tRNA is hydrolyzed during electrophoresis, but most remains attached. Treatment with puromycin hydrolyzes the tRNA, resulting in translocation of the polypeptide as judged by signal peptide cleavage. The cleaved FLAG-tagged signal is weakly visible due to its single radiolabeled methionine. (C) Microsomes containing the 86-mer translocation intermediate of FLAG-pPL or untagged pPL were isolated by centrifugation, solubilized with digitonin-containing buffer, and subjected to affinity purification via the FLAG tag. The eluted products were analyzed for recovery of Sec61 complex by immunoblotting relative to serial dilutions of starting microsomes. Sec61 complex is recovered only with the tagged substrate, indicating specificity of its recovery. (D) Immunoblotting of affinity

purified FLAG-pPL 86-mer complexes (as in panel C) for Sec61 and ribosomal proteins show that they are recovered at a ratio comparable to that observed in the starting rough microsomes.

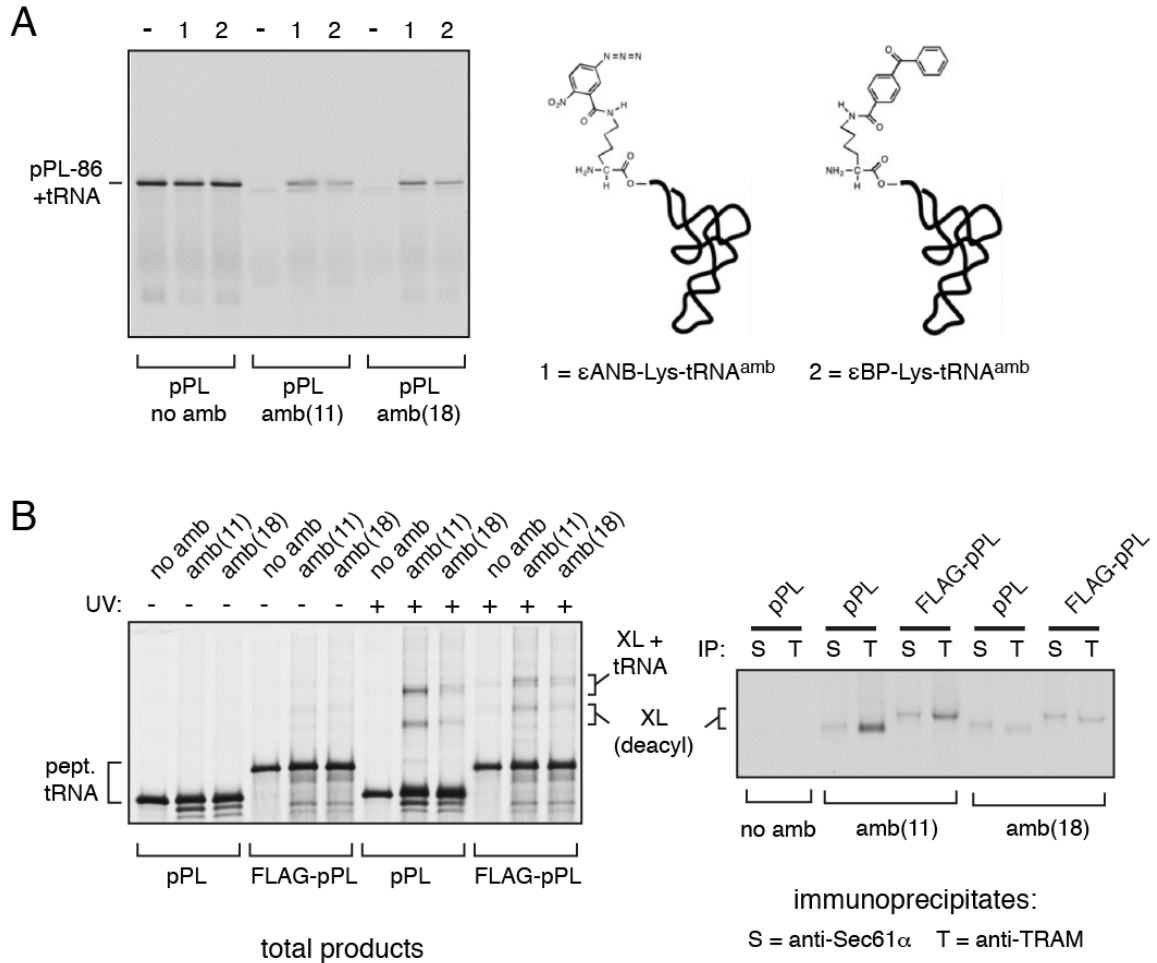


Fig. S3. Analysis of signal peptide interactions by site-specific cross-linking. (A) Amber codons at positions 11 or 18 were introduced into the pPL signal peptide. The 86-mer intermediate of the unmutated or amber-containing constructs was translated in vitro with 35 S-methionine and one of two charged amber-suppressor tRNAs whose structures are shown. Note that full length translation product (represented by the 86-mer peptidyl-tRNA) is not produced when amber codons are present unless also suppressed by either of the two tRNAs. Suppression efficiencies are ~10-25%. This permits incorporation of the indicated unnatural amino acids, both suitable for photo-cross-linking, at defined positions. (B) The indicated 86-mer peptidyl-tRNA intermediates of pPL or FLAG-pPL constructs were assembled on rough microsomes as in Fig. S2B. The constructs contained amber codons at the indicated positions, and the translation reactions contained the ϵ ANB-Lys-tRNA^{amb} suppressor tRNA for incorporation of photo-cross-linker. The microsomes were isolated by centrifugation, divided in two, and one half subjected to UV irradiation for 15 min to induce photo-cross-linking. An aliquot of the total products was analyzed (left panel), while the remainder was subjected to denaturing immunoprecipitation (IP) using antibodies against either Sec61 α or TRAM (right panel). The left panel shows the position of the uncross-linked peptidyl-tRNA products, and the major cross-linked species. Partial deacylation of the tRNA occurs during electrophoresis, resulting in two major cross-linked bands. The IPs show that the cross-

linked band (which becomes fully deacylated during the IP) is a mixture of Sec61 α and TRAM. The overall cross-linking efficiency and the ratio of Sec61 to TRAM cross-links vary depending on cross-linker position [10-13]. The pattern of both efficiency and ratio is the same for pPL and FLAG-pPL, strongly arguing that the two signals are positioned in the translocon in very similar ways. Similar concordance was also seen for the other cross-linker (not shown).

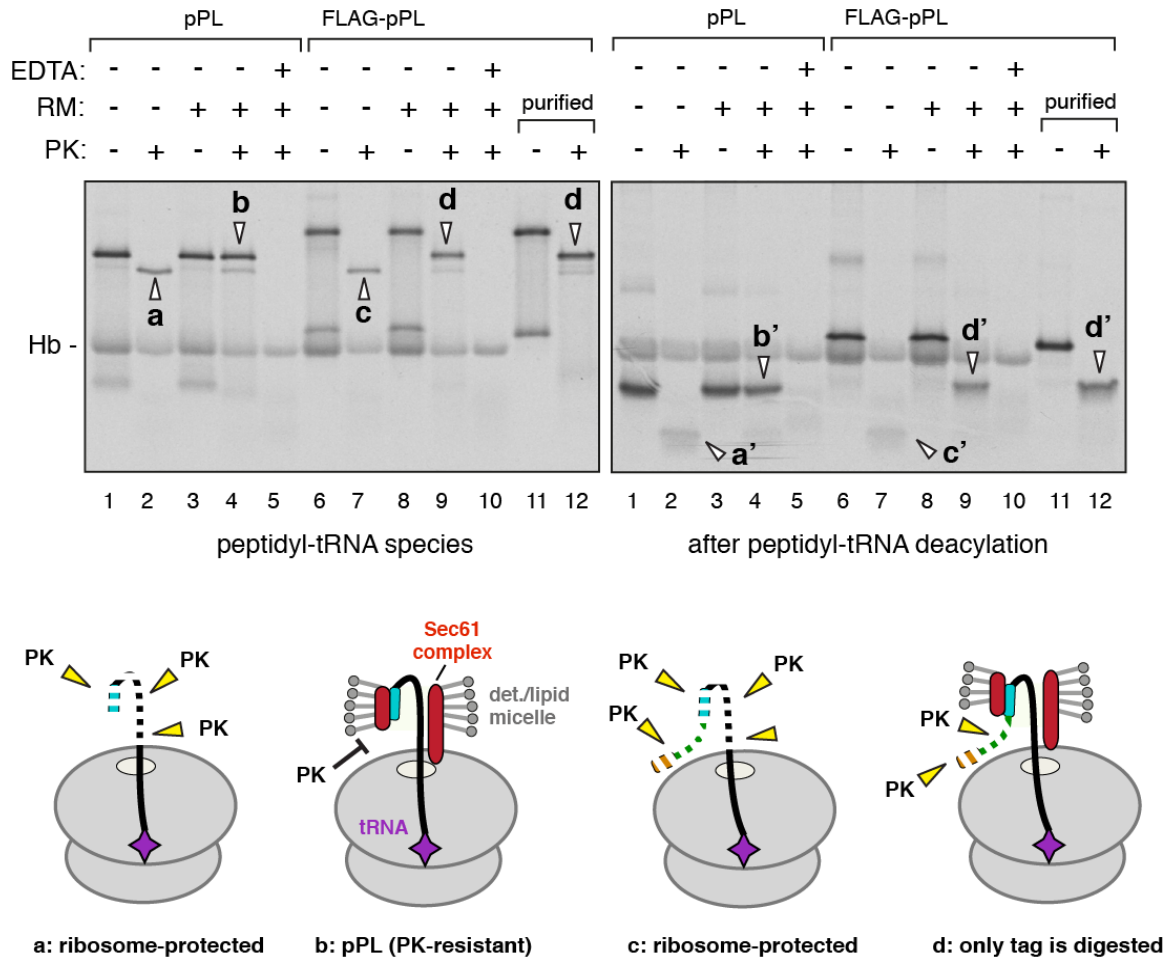


Fig. S4. Analysis of nascent chain engagement of Sec61 by protease protection. 86-mer peptidyl-tRNA translocation intermediates of either pPL or FLAG-pPL were translated with ³⁵S-methionine as in Fig. S2B in reactions that either lacked or contained rough microsomes (RM). One aliquot of the RM-targeted FLAG-pPL sample was solubilized and affinity purified using conditions identical to those for structure determination (lanes 11, 12), while the remaining samples were analyzed directly after adjusting them with 1% digitonin to dissolve the membrane. Aliquots were treated with proteinase K (PK) in the absence or presence of EDTA to disrupt the ribosome where indicated. The samples were analyzed directly to visualize the peptidyl-tRNA species (left gel) or after high pH induced hydrolysis of the tRNA (right gel). Key molecular species (a-d) are indicated with arrowheads, and the interpretations of these respective products are shown in the four diagrams under the gel. Species a' to d' are the deacylated versions of species a to d, respectively. Hb indicates haemoglobin, produced and/or labeled at low levels in the reticulocyte-based translation extract. As expected, PK digestion of pPL or FLAG-pPL in the absence of RM produces a short tRNA-attached fragment with ~35-40 residues protected by the ribosomal tunnel (lanes 2 and 7; species a and c). In the presence of RM, pPL is now fully protected due to its insertion into the Sec61 translocon (lane 4, species b) as shown previously [12]. By contrast, FLAG-pPL is partially protected, resulting in a tRNA-attached fragment whose size is identical to the fully protected pPL 86-mer (lane 9, species d). Thus, the FLAG tag and linker extension

are accessible to protease, while the native pPL portion of the nascent chain is shielded similarly to untagged pPL (compare diagrams b and d). This identical pattern of PK accessibility is retained on samples after they have undergone affinity purification (lane 12, compare to lane 9), strongly suggesting that nascent chain insertion into the Sec61 translocon is not disrupted by the purification process.

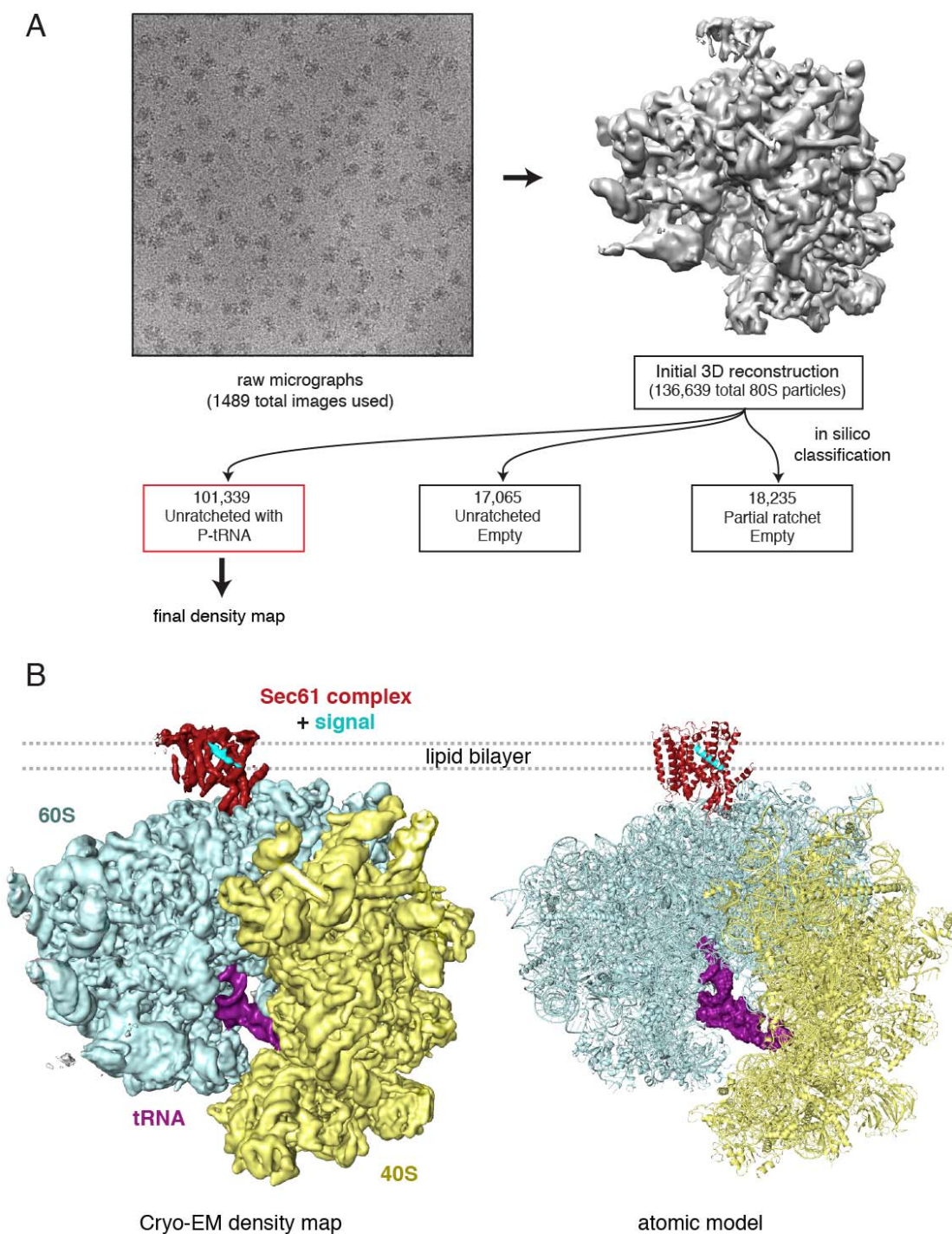


Fig. S5. Overview of particle classification and structure determination. (A) Schematic of the data collection and particle classification scheme used to derive the final density map. Note that the initial 3D reconstruction of all particles from down-sampled micrographs without movie processing or particle polishing already shows very clear density for the Sec61 complex in which individual transmembrane helices are readily visible, including the signal peptide. At this threshold, the detergent micelle surrounding

the Sec61 complex is not visible due to its heterogeneity relative to the homogeneous and defined positions of the transmembrane helices of the Sec61 complex (and of course, the ribosome). From this total particle dataset, in silico classification was used to identify the ~74% of particles containing an unrathected ribosome and P-site tRNA, which was used as a surrogate to identify those particles containing a nascent chain. This subset was used to produce the final density map. **(B)** The unsharpened EM density map (left panel) is shown with the final molecular model (right panel). The components are colored as follows: 40S subunit (yellow), 60S subunit (blue), the peptidyl-tRNA (purple), the Sec61 channel (red), and the signal peptide (cyan). Note that this is the raw density map shown at a single threshold without any segmentation. At the displayed threshold where each of the individual transmembrane helices of the Sec61 complex and the signal peptide are clearly visible and resolved, the detergent-lipid micelle is not observed. Thus, the occupancy and homogeneity of the signal-Sec61 complex is very high, suggesting that it represents a single uniform conformation.

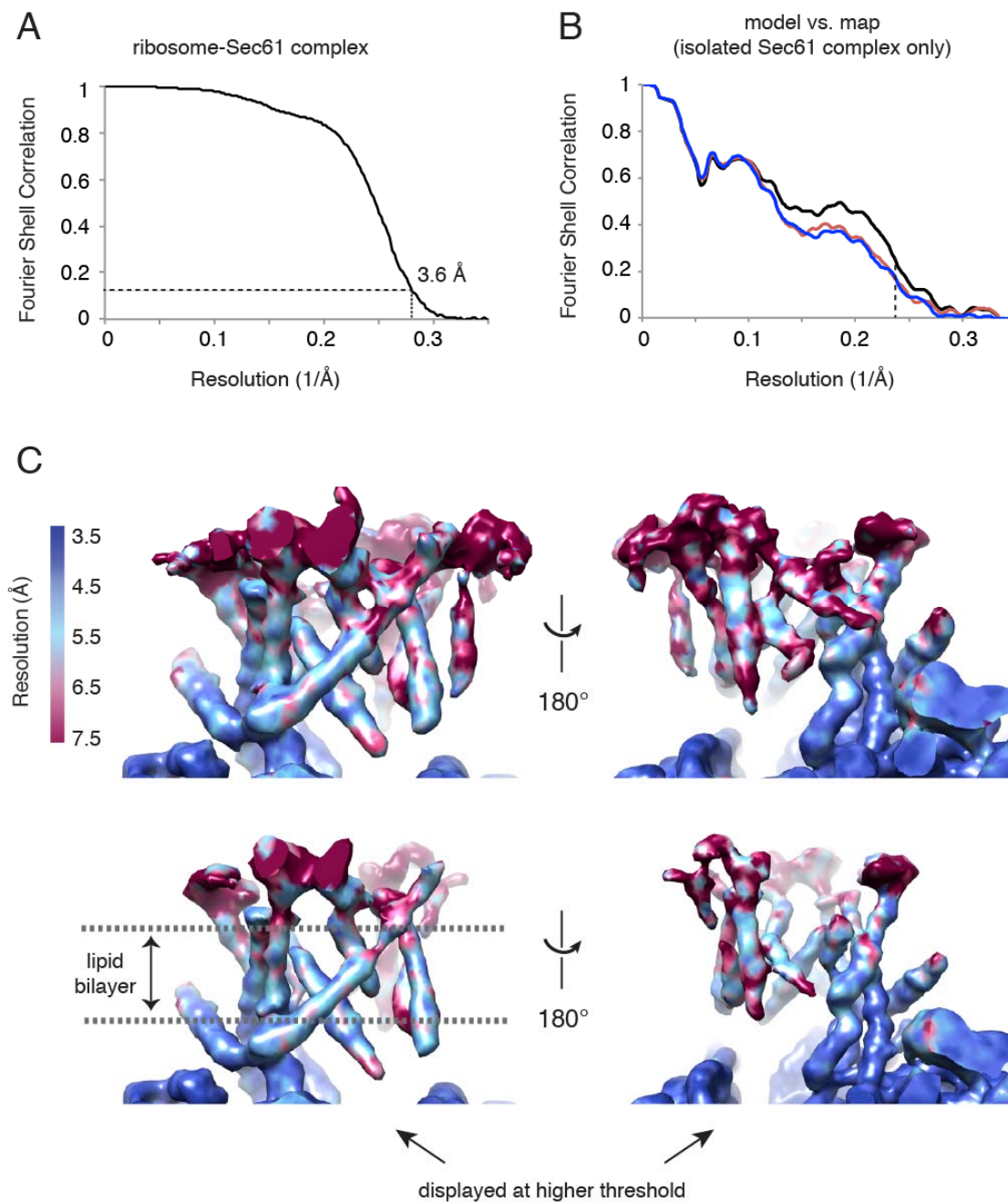


Fig. S6. Map and model quality. (A) Gold-standard Fourier Shell Correlation (FSC) curve for the map of the engaged ribosome-Sec61 complex where the overall resolution is demarcated using the FSC=0.143 criterion. (B) FSC curves for the isolated Sec61 region of the map. The curve for the final model versus the map derived from the complete dataset is shown in black; red shows the curve for a model refined in the first of two independent halves of the map; and blue shows that same model versus the second independent half-map, which was not used for refinement. The vertical dashed line indicates the highest resolution (4.25 \AA) used in these model refinements. (C) Local resolution of the engaged channel, produced using ResMap [44], shown from either the Sec61 γ side (left) or lateral gate (right). Two different thresholds are displayed in the

upper and lower panels. The resolution of the Sec61 regions contacting the ribosome approach ~ 3.5 Å resolution, while the flexible loops on the luminal side of Sec61 are ~ 7 Å. In regions of Sec61 that are in the membrane (demarcated in the lower-left panel), most of the TM helices range between ~ 4.0 - 5.5 Å resolution.

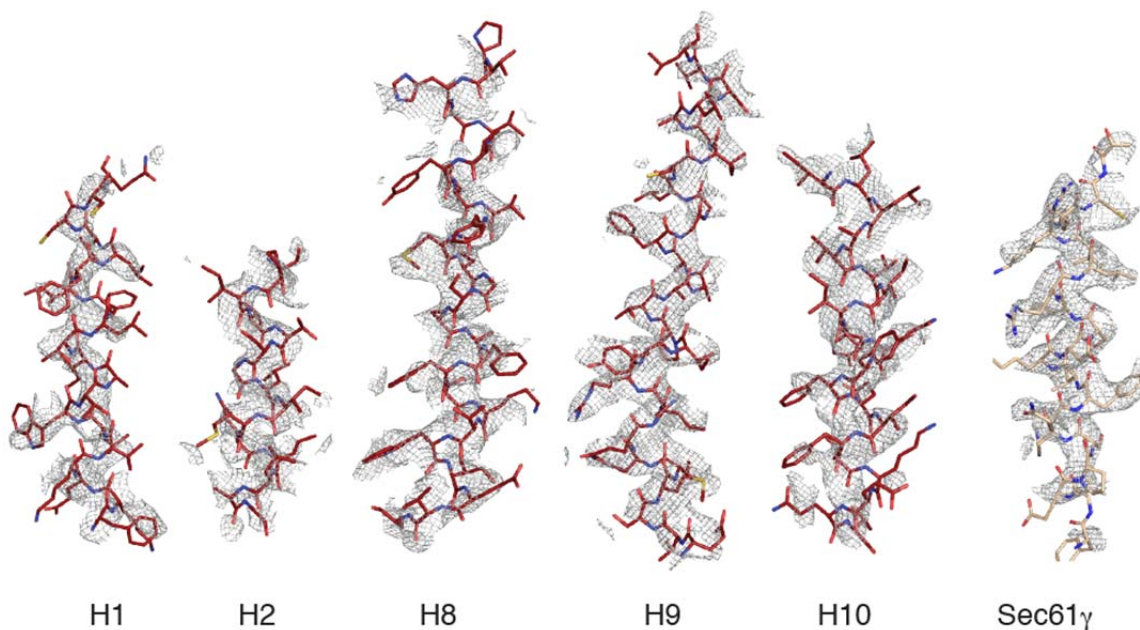


Fig. S7. Examples of map quality. Representative density from sharpened maps for several of the TM helices from the Sec61 complex, filtered to 3.8 Å, and their associated molecular models. The quality of the data is such that placement of the helix and the helical pitch is unambiguous for all helices in the channel, while many amino acid side chains are visible in both the stationary (helices 6-9, γ) and mobile (1-5,10, β) portions of Sec61.

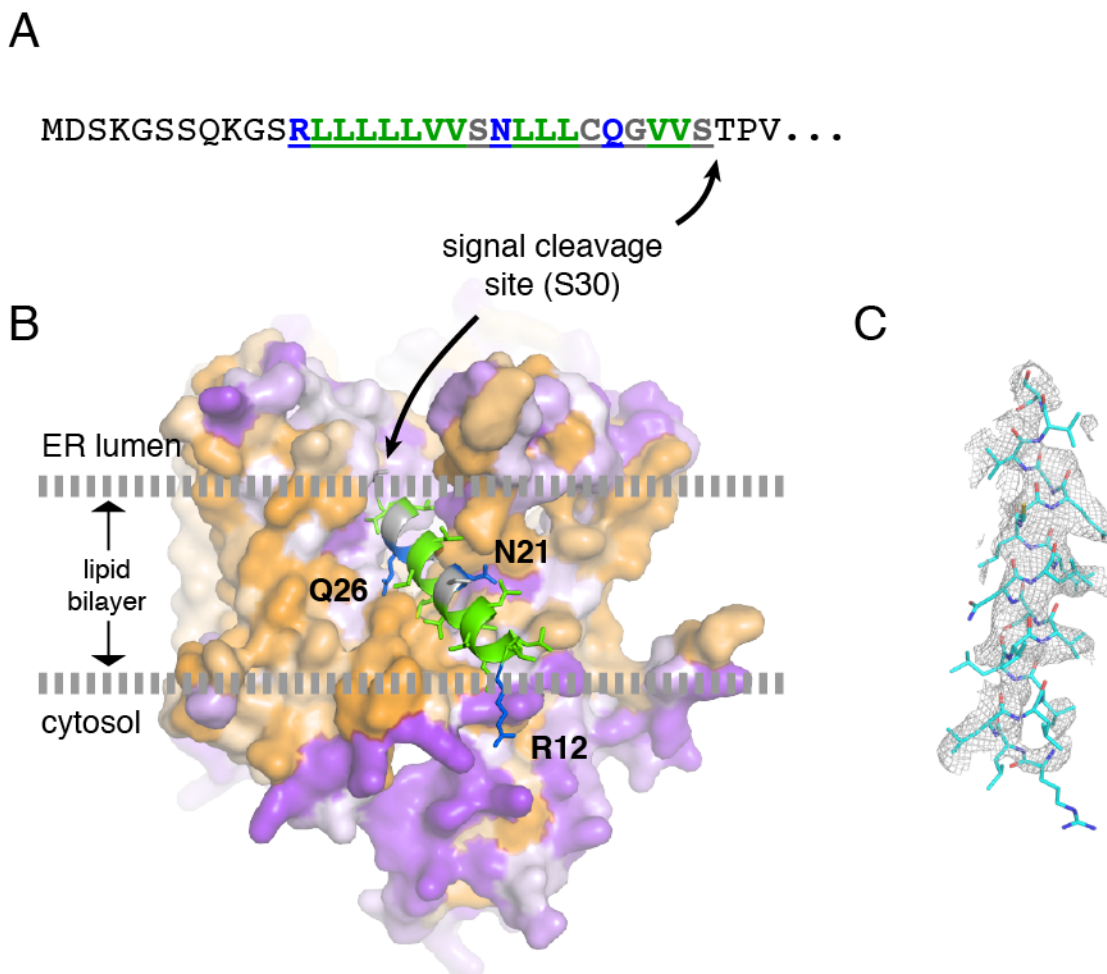


Fig. S8. Assignment of a likely registry for the signal peptide relative to Sec61. The sequence of the pPL signal peptide is shown, with the region modelled in our map underlined. Highly hydrophilic/polar residues are indicated in blue, while highly hydrophobic residues are green. The position of signal cleavage is indicated. **(A)** Signal sequence. **(B)** Shown is a space filling model of the engaged Sec61 complex colored by hydrophobicity, with orange indicating hydrophobic and purple hydrophilic surfaces. The signal sequence helix is shown with sticks for side chains, colored using the same scheme as in **(A)**. The three particularly hydrophilic residues are unlikely to be facing lipid or the hydrophobic surface of Sec61. Hence, a registry was chosen that not only best matches with the density map **(C)**, but also one in which hydrophilic residues can either snorkel to the lipid head groups (R12) or face hydrophilic regions on Sec61 (N21 and Q26). Conversely, the hydrophobic residues primarily face either lipid or hydrophobic Sec61 surfaces. Finally, the signal peptide cleavage site is likely to be at the luminal side of the lipid bilayer, since it will eventually be accessed by signal peptidase whose active site is in the lumen. Conversely, the sequences preceding R12 (not modelled) are likely to be facing the cytosol and outside the lipid bilayer given their high hydrophilicity. Thus, the chosen registry fits best with known biological activities (site of signal cleavage and n-region facing the cytosol) as well as biophysical considerations. Other registries for the signal peptide either did not fit as well into the density map or resulted in unfavorable

hydrophobic mismatch. **(C)** The density map for the modelled region of the signal peptide (grey mesh) shown with the final atomic model (cyan) as in Fig. S7.

Table S1. Refinement and model statistics.

Data collection	
Particles	101,339
Pixel size (Å)	1.34
Defocus range (mm)	2.0-3.5
Voltage (kV)	300
Electron dose (e/Å ²)	27
Map sharpening B-factor (Å ²)	-72.6
Model composition	Engaged Sec61
Non-hydrogen atoms	3,912
Protein residues	514
Refinement	
Resolution used (Å)	4.25
Average B factor (Å ²)	156
Fourier shell correlation (FSC)*	0.72
Rms deviations	
Bonds (Å)	0.011
Angles (°)	1.5
Ramachandran plot	
Favored (%)	94
Outliers (%)	6

$$*FSC = \frac{\sum(F_{obs} F_{calc}^*)}{\sqrt{(\sum|F_{obs}|^2 \sum|F_{calc}|^2)}}$$

Table S2. Conserved residues of key functional motifs.

Motif	<i>H. sapiens</i> residues	<i>M. jannaschii</i> residues
Polar Cluster	T86	T80
	Q127	E122
	N300	N268
	I81	I75
	V85	V79
Pore ring	I179	I170
	I183	I174
	I292	I260
	L449	L406
	V85	V79
Hydrophobic patch	L89	I83
	I179	I170
	I293	L261

Movie S1. Morph between the ribosome-primed idle Sec61 complex (3J7Q) and the engaged Sec61 complex. The view is from the plan of the membrane looking toward the lateral gate; the ribosome would be on the bottom and ER lumen on the top. Only the transmembrane segments and the ribosome-interacting cytosolic loops are shown for clarity. Sec61 α , β , and γ are in red, light blue, and tan, respectively. The signal sequence (cyan) appears in the engaged state at its position in the lateral gate.

Movie S2. Morph between the ribosome-primed idle Sec61 complex (3J7Q) and the engaged Sec61 complex as viewed from the ER lumen. The lateral gate is on the bottom. Only the transmembrane segments are depicted for clarity. At the beginning of the animation, Sec61 α , β , and γ are in red, light blue, and tan, respectively. The helices that rotate as a rigid body turn grey just before their movement. The signal sequence (cyan) appears in the engaged state at the end of the animation.

REFERENCES AND NOTES

1. E. Park, T. A. Rapoport, Mechanisms of Sec61/SecY-mediated protein translocation across membranes. *Annu. Rev. Biophys.* **41**, 21–40 (2012). [Medline](#) [doi:10.1146/annurev-biophys-050511-102312](https://doi.org/10.1146/annurev-biophys-050511-102312)
2. B. Van den Berg, W. M. Clemons Jr., I. Collinson, Y. Modis, E. Hartmann, S. C. Harrison, T. A. Rapoport, X-ray structure of a protein-conducting channel. *Nature* **427**, 36–44 (2004). [Medline](#) [doi:10.1038/nature02218](https://doi.org/10.1038/nature02218)
3. K. Plath, W. Mothes, B. M. Wilkinson, C. J. Stirling, T. A. Rapoport, Signal sequence recognition in posttranslational protein transport across the yeast ER membrane. *Cell* **94**, 795–807 (1998). [Medline](#) [doi:10.1016/S0092-8674\(00\)81738-9](https://doi.org/10.1016/S0092-8674(00)81738-9)
4. P. F. Egea, R. M. Stroud, Lateral opening of a translocon upon entry of protein suggests the mechanism of insertion into membranes. *Proc. Natl. Acad. Sci. U.S.A.* **107**, 17182–17187 (2010). [Medline](#) [doi:10.1073/pnas.1012556107](https://doi.org/10.1073/pnas.1012556107)
5. T. Tsukazaki, H. Mori, S. Fukai, R. Ishitani, T. Mori, N. Dohmae, A. Perederina, Y. Sugita, D. G. Vassylyev, K. Ito, O. Nureki, Conformational transition of Sec machinery inferred from bacterial SecYE structures. *Nature* **455**, 988–991 (2008). [Medline](#) [doi:10.1038/nature07421](https://doi.org/10.1038/nature07421)
6. J. Zimmer, Y. Nam, T. A. Rapoport, Structure of a complex of the ATPase SecA and the protein-translocation channel. *Nature* **455**, 936–943 (2008). [Medline](#) [doi:10.1038/nature07335](https://doi.org/10.1038/nature07335)
7. M. Gogala, T. Becker, B. Beatrix, J. P. Armache, C. Barrio-Garcia, O. Berninghausen, R. Beckmann, Structures of the Sec61 complex engaged in nascent peptide translocation or membrane insertion. *Nature* **506**, 107–110 (2014). [Medline](#) [doi:10.1038/nature12950](https://doi.org/10.1038/nature12950)
8. E. Park, J. F. Ménétret, J. C. Gumbart, S. J. Ludtke, W. Li, A. Whynot, T. A. Rapoport, C. W. Akey, Structure of the SecY channel during initiation of protein translocation. *Nature* **506**, 102–106 (2014). [Medline](#) [doi:10.1038/nature12720](https://doi.org/10.1038/nature12720)
9. R. M. Voorhees, I. S. Fernández, S. H. W. Scheres, R. S. Hegde, Structure of the mammalian ribosome-Sec61 complex to 3.4 Å resolution. *Cell* **157**, 1632–1643 (2014). [Medline](#) [doi:10.1016/j.cell.2014.05.024](https://doi.org/10.1016/j.cell.2014.05.024)
10. S. High *et al.*, Site-specific photocross-linking reveals that Sec61p and TRAM contact different regions of a membrane-inserted signal sequence. *J. Biol. Chem.* **268**, 26745–26751 (1993). [Medline](#)
11. W. Mothes, S. Prehn, T. A. Rapoport, Systematic probing of the environment of a translocating secretory protein during translocation through the ER membrane. *EMBO J.* **13**, 3973–3982 (1994). [Medline](#)
12. B. Jungnickel, T. A. Rapoport, A posttargeting signal sequence recognition event in the endoplasmic reticulum membrane. *Cell* **82**, 261–270 (1995). [Medline](#) [doi:10.1016/0092-8674\(95\)90313-5](https://doi.org/10.1016/0092-8674(95)90313-5)
13. W. Mothes, B. Jungnickel, J. Brunner, T. A. Rapoport, Signal sequence recognition in cotranslational translocation by protein components of the endoplasmic reticulum

- membrane. *J. Cell Biol.* **142**, 355–364 (1998). [Medline doi:10.1083/jcb.142.2.355](#)
14. K. S. Crowley, S. Liao, V. E. Worrell, G. D. Reinhart, A. E. Johnson, Secretory proteins move through the endoplasmic reticulum membrane via an aqueous, gated pore. *Cell* **78**, 461–471 (1994). [Medline doi:10.1016/0092-8674\(94\)90424-3](#)
 15. B. Martoglio, M. W. Hofmann, J. Brunner, B. Dobberstein, The protein-conducting channel in the membrane of the endoplasmic reticulum is open laterally toward the lipid bilayer. *Cell* **81**, 207–214 (1995). [Medline doi:10.1016/0092-8674\(95\)90330-5](#)
 16. S. Pfeffer, L. Burbaum, P. Unverdorben, M. Pech, Y. Chen, R. Zimmermann, R. Beckmann, F. Förster, Structure of the native Sec61 protein-conducting channel. *Nat. Commun.* **6**, 8403 (2015). [10.1038/ncomms9403](#) [Medline doi:10.1038/ncomms9403](#)
 17. Although P-site transfer RNA was absent from the majority of ribosomes used for the cryo-tomography structure (*16*), the presence or absence of heterogeneous endogenous nascent polypeptides within Sec61 could not be determined conclusively. Thus, the conclusion that the Sec61 complex is constitutively open upon ribosome binding, independent of substrate or functional state, may be premature. Indeed, biochemical studies in native microsomes show substrate-induced Sec61 opening (*14*), no translocation of Sec61-docked polypeptides with a mutant signal (*12*), and no lipid access to early translocation intermediates (*13*). Genetic studies show that modulation of lateral gate interactions influences translocation (*20–27*). Thus, multiple independent findings argue that substrates induce structural changes to the Sec61 complex that open it laterally.
 18. R. M. Voorhees, R. S. Hegde, Structures of the scanning and engaged states of the mammalian SRP-ribosome complex. *eLife* **4**, e07975 (2015). [Medline doi:10.7554/eLife.07975](#)
 19. K. S. Crowley, G. D. Reinhart, A. E. Johnson, The signal sequence moves through a ribosomal tunnel into a noncytoplasmic aqueous environment at the ER membrane early in translocation. *Cell* **73**, 1101–1115 (1993). [Medline doi:10.1016/0092-8674\(93\)90640-C](#)
 20. T. Junne, T. Schwede, V. Goder, M. Spiess, Mutations in the Sec61p channel affecting signal sequence recognition and membrane protein topology. *J. Biol. Chem.* **282**, 33201–33209 (2007). [Medline doi:10.1074/jbc.M707219200](#)
 21. M. A. Smith, W. M. J. Clemons Jr., C. J. DeMars, A. M. Flower, Modeling the effects of *prl* mutations on the *Escherichia coli* SecY complex. *J. Bacteriol.* **187**, 6454–6465 (2005). [Medline doi:10.1128/JB.187.18.6454-6465.2005](#)
 22. A. I. Derman, J. W. Puziss, P. J. J. Bassford Jr., J. Beckwith, A signal sequence is not required for protein export in *prlA* mutants of *Escherichia coli*. *EMBO J.* **12**, 879–888 (1993). [Medline](#)
 23. R. S. Osborne, T. J. Silhavy, *PrlA* suppressor mutations cluster in regions corresponding to three distinct topological domains. *EMBO J.* **12**, 3391–3398

- (1993). [Medline](#)
24. A. P. Maillard, S. Lalani, F. Silva, D. Belin, F. Duong, Deregulation of the SecYEG translocation channel upon removal of the plug domain. *J. Biol. Chem.* **282**, 1281–1287 (2007). [Medline doi:10.1074/jbc.M610060200](#)
 25. S. F. Trueman, E. C. Mandon, R. Gilmore, A gating motif in the translocation channel sets the hydrophobicity threshold for signal sequence function. *J. Cell Biol.* **199**, 907–918 (2012). [Medline doi:10.1083/jcb.201207163](#)
 26. A. L. Mackinnon, V. O. Paavilainen, A. Sharma, R. S. Hegde, J. Taunton, An allosteric Sec61 inhibitor traps nascent transmembrane helices at the lateral gate. *eLife* **3**, e01483 (2014). [Medline doi:10.7554/eLife.01483](#)
 27. T. Junne, J. Wong, C. Studer, T. Aust, B. W. Bauer, M. Beibel, B. Bhullar, R. Brucoleri, J. Eichenberger, D. Estoppey, N. Hartmann, B. Knapp, P. Krastel, N. Melin, E. J. Oakeley, L. Oberer, R. Riedl, G. Roma, S. Schuierer, F. Petersen, J. A. Tallarico, T. A. Rapoport, M. Spiess, D. Hoepfner, Decatransin, a new natural product inhibiting protein translocation at the Sec61/SecYEG translocon. *J. Cell Sci.* **128**, 1217–1229 (2015). [Medline doi:10.1242/jcs.165746](#)
 28. S. Shao, K. von der Malsburg, R. S. Hegde, Listerin-dependent nascent protein ubiquitination relies on ribosome subunit dissociation. *Mol. Cell* **50**, 637–648 (2013). [Medline doi:10.1016/j.molcel.2013.04.015](#)
 29. S. Shao, R. S. Hegde, Reconstitution of a minimal ribosome-associated ubiquitination pathway with purified factors. *Mol. Cell* **55**, 880–890 (2014). [Medline doi:10.1016/j.molcel.2014.07.006](#)
 30. R. D. Fons, B. A. Bogert, R. S. Hegde, Substrate-specific function of the translocon-associated protein complex during translocation across the ER membrane. *J. Cell Biol.* **160**, 529–539 (2003). [Medline doi:10.1083/jcb.200210095](#)
 31. A. Sharma, M. Mariappan, S. Appathurai, R. S. Hegde, In vitro dissection of protein translocation into the mammalian endoplasmic reticulum. *Methods Mol. Biol.* **619**, 339–363 (2010). [Medline doi:10.1007/978-1-60327-412-8_20](#)
 32. P. Walter, G. Blobel, Preparation of microsomal membranes for cotranslational protein translocation. *Methods Enzymol.* **96**, 84–93 (1983). [Medline doi:10.1016/S0076-6879\(83\)96010-X](#)
 33. S. J. Kim, R. S. Hegde, Cotranslational partitioning of nascent prion protein into multiple populations at the translocation channel. *Mol. Biol. Cell* **13**, 3775–3786 (2002). [Medline doi:10.1091/mbc.E02-05-0293](#)
 34. D. Görlich, T. A. Rapoport, Protein translocation into proteoliposomes reconstituted from purified components of the endoplasmic reticulum membrane. *Cell* **75**, 615–630 (1993). [Medline doi:10.1016/0092-8674\(93\)90483-7](#)
 35. X.-C. Bai, I. S. Fernandez, G. McMullan, S. H. W. Scheres, Ribosome structures to near-atomic resolution from thirty thousand cryo-EM particles. *eLife* **2**, e00461 (2013). [Medline doi:10.7554/eLife.00461](#)
 36. J. A. Mindell, N. Grigorieff, Accurate determination of local defocus and specimen

- tilt in electron microscopy. *J. Struct. Biol.* **142**, 334–347 (2003). [Medline](#)
[doi:10.1016/S1047-8477\(03\)00069-8](https://doi.org/10.1016/S1047-8477(03)00069-8)
37. S. H. W. Scheres, RELION: Implementation of a Bayesian approach to cryo-EM structure determination. *J. Struct. Biol.* **180**, 519–530 (2012). [Medline](#)
[doi:10.1016/j.jsb.2012.09.006](https://doi.org/10.1016/j.jsb.2012.09.006)
38. S. H. Scheres, Beam-induced motion correction for sub-megadalton cryo-EM particles. *eLife* **3**, e03665 (2014). [Medline](#) [doi:10.7554/eLife.03665](https://doi.org/10.7554/eLife.03665)
39. S. H. W. Scheres, S. Chen, Prevention of overfitting in cryo-EM structure determination. *Nat. Methods* **9**, 853–854 (2012). [Medline](#)
[doi:10.1038/nmeth.2115](https://doi.org/10.1038/nmeth.2115)
40. G. N. Murshudov, P. Skubák, A. A. Lebedev, N. S. Pannu, R. A. Steiner, R. A. Nicholls, M. D. Winn, F. Long, A. A. Vagin, REFMAC5 for the refinement of macromolecular crystal structures. *Acta Crystallogr. D Biol. Crystallogr.* **67**, 355–367 (2011). [Medline](#) [doi:10.1107/S0907444911001314](https://doi.org/10.1107/S0907444911001314)
41. A. Amunts, A. Brown, X. C. Bai, J. L. Llácer, T. Hussain, P. Emsley, F. Long, G. Murshudov, S. H. Scheres, V. Ramakrishnan, Structure of the yeast mitochondrial large ribosomal subunit. *Science* **343**, 1485–1489 (2014). [Medline](#)
[doi:10.1126/science.1249410](https://doi.org/10.1126/science.1249410)
42. A. Brown, F. Long, R. A. Nicholls, J. Toots, P. Emsley, G. Murshudov, Tools for macromolecular model building and refinement into electron cryo-microscopy reconstructions. *Acta Crystallogr. D Biol. Crystallogr.* **71**, 136–153 (2015).
[Medline](#) [doi:10.1107/S1399004714021683](https://doi.org/10.1107/S1399004714021683)
43. R. A. Nicholls, F. Long, G. N. Murshudov, Low-resolution refinement tools in REFMAC5. *Acta Crystallogr. D Biol. Crystallogr.* **68**, 404–417 (2012). [Medline](#)
[doi:10.1107/S090744491105606X](https://doi.org/10.1107/S090744491105606X)
44. A. Kucukelbir, F. J. Sigworth, H. D. Tagare, Quantifying the local resolution of cryo-EM density maps. *Nat. Methods* **11**, 63–65 (2014). [Medline](#)
[doi:10.1038/nmeth.2727](https://doi.org/10.1038/nmeth.2727)
45. W. L. DeLano, *The PyMOL Molecular Graphics System* (DeLano Scientific, Palo Alto, CA, 2006); www.pymol.org.
46. T. D. Goddard, C. C. Huang, T. E. Ferrin, Visualizing density maps with UCSF Chimera. *J. Struct. Biol.* **157**, 281–287 (2007). [Medline](#)
[doi:10.1016/j.jsb.2006.06.010](https://doi.org/10.1016/j.jsb.2006.06.010)